

Heavy Residue Formation in 20 MeV/nucleon $^{197}\text{Au} + ^{90}\text{Zr}$ Collisions

G.A. Souliotis^{a,1}, W. Loveland^a, K. Hanold^{b,2},
G.J. Wozniak^c, and D.J. Morrissey^d.

^a*Dept. of Chemistry, Oregon State University, Corvallis, OR 97331.*

^b*Dept. of Chemistry, Univ. of California, San Diego, La Jolla, CA 92093.*

^c*Lawrence Berkeley National Laboratory, Univ. of California,
Berkeley, CA 94720.*

^d*National Superconducting Cyclotron Laboratory, Michigan State
University, East Lansing, MI 48824.*

Abstract

The yields and velocity distributions of heavy residues and fission fragments from the reaction of 20 MeV/nucleon $^{197}\text{Au} + ^{90}\text{Zr}$ have been measured using the MSU A1200 fragment separator. A bimodal distribution of residues is observed, with one group, resulting from peripheral collisions, having fragment mass numbers $A=160-200$ while the other group, resulting from “hard” collisions, has $A=120-160$. This latter group of residues can be distinguished from fission fragments by their lower velocities. A model combining deep-inelastic transfer and incomplete fusion for the primary interaction stage and a statistical evaporation code for the deexcitation stage has been used to describe the properties of the product distributions.

Key words: Nuclear reactions, incomplete fusion, deep inelastic scattering
PACS: 25.70.-z, 25.70.Jj, 25.70.Lm

1 Introduction

The yields of the heavy residues [1,2], i.e., the large remnants of the heavy member of an asymmetric reacting pair of nuclei, are known to comprise a

¹ Corresponding author: soulioti@comp.tamu.edu. Current Address: Cyclotron Institute, Texas A&M Univ., College Station, TX 77843.

² Current address: Syagen Technology, 1411 Warner Ave., Tustin, CA 92780.

large fraction of the reaction cross section for intermediate energy nuclear collisions. However, there are experimental difficulties in studying the formation of these nuclei in asymmetric reactions using “normal” kinematics. The energies of the residues are low (~ 15 keV/nucleon [1,2]) and the masses are large. Experimental thresholds cause one to miss substantial portions (50%) of the product distributions [1]. One can overcome the problem of detecting low fragment energies by studying these asymmetric reactions in “inverse kinematics”, i.e., bombard a low mass nucleus with a large mass nucleus. By using a high resolution spectrometer/detector system to observe the projectile-like fragments (PLFs) from such reactions, one can gain important information about the reaction mechanism, complementary to that obtained in exclusive studies, where only the light reaction partners are observed with high isotopic resolution.

Pioneering studies by Bazin, et al.[3], Faure-Ramstein, et al. [4], Pfaff, et al. [5] and Hanold, et al. [6] have shown the utility of this approach in studying the heavy reaction products from Kr+X and Xe+X mass asymmetric collisions at intermediate energies. In a previous paper [7], we reported the results of a similar study of the reaction of 20 MeV/nucleon ^{197}Au with the light nuclei ^{12}C and ^{27}Al . In these cases, we focussed on *fusion-like events* and tried to understand the details of the particle emission/fission competition in the de-excitation of these hot nuclei. In this paper, we report the results of an extension of the previous work to study the yields and velocities of the heavy residues and fission fragments from the interaction of ^{197}Au (20 MeV/nucleon) with an intermediate mass nucleus, ^{90}Zr . In these systems, fusion-like collisions are less frequent. Previous studies [3,8–12], [13–16] of the collisions of heavier nuclei at intermediate energies have shown binary dissipative collisions to be the dominant reaction mechanism. Evidence has been presented [16] for a sequential decay of one of the initial binary fragments leading to a three (or more) body final state along with dynamically emitted IMFs from the collision complex [17]. In some of the binary encounters the projectile-like fragments have been found [12,15] to have very high temperatures ($T\sim 7$ MeV). A variety of phenomenological models have been used, with modest success, to describe these collisions [10,11,13]. The goal of this extension of previous work is to understand quantitatively the reaction mechanism(s) responsible for residue formation in more symmetric collisions at 20 MeV/nucleon. We shall present evidence indicating that, in addition to the traditional evaporation residues from peripheral collisions, some residues are formed in “hard” collisions, possibly resulting from very asymmetric fission and/or IMF emission. The distributions of these residues, which are very proton-rich, cannot be fully described by available phenomenological models of these collisions.

Although the Au + Zr reaction has not, to the best of our knowledge, been studied before, there are a large number of studies [18–27], [28–36] of the analogous $^{197}\text{Au} + \text{Kr}$ reaction at intermediate energies ranging from 4.9 to

70 MeV/nucleon with some studies [21,23,24,28] at a beam energy of ~ 20 MeV/nucleon. What this work adds to this extensive data set is detailed, high resolution information on the properties of the heavy, Au-like fragments in these reactions garnered from physical rather than radiochemical measurements. (The previous studies of the Kr + Au reaction generally point to the presence of both deep inelastic and fusion-like mechanisms. The fragments of Au arise as both fission fragments and evaporation residues [33,35] with the residues being formed in collisions involving a larger dissipation of the projectile energy.)

The paper is organized as follows: In Section 2, a brief description of the experimental apparatus, the measurements and the data analysis is given. In Section 3, yield distributions are presented and compared with previous work. Also the velocity distributions are discussed. In Section 4, the results of the measurements are compared to modern models of the dissipative features of intermediate energy collisions. Finally, conclusions from the present study are summarized in Section 5.

2 Experimental

2.1 Description of Apparatus

The experiment was performed at the National Superconducting Cyclotron Laboratory at Michigan State University using the A1200 fragment separator [37]. This work is a direct extension of the work of Souliotis et al. [7], where the collisions of 20 MeV/nucleon ^{197}Au with C and Al were studied. It should be noted that use of the A1200 for very asymmetric collisions with heavy beams (where the grazing angle is small, i.e. $1-2^\circ$ [38]), leads to rather efficient collection of the projectile residues (that can reach 50%) at this energy regime. However, using the A1200 for more symmetric systems, as for the Au+Zr reaction in this work (where the grazing angle is 5.5°), results in substantial loss of residue cross sections, since the measurements are performed near 0° , while the residue cross sections are expected to peak at larger angles, close to the grazing angle. In this case, only a small fraction of the residue cross section can be collected (of the order of a few percent). Despite this limitation, we attempted to exploit the possibility of getting isotopically resolved Au fragments with this apparatus and tried to extract some information regarding the production mechanism. The experimental setup, calibration procedures and data analysis were similar as in ref. [7] and are briefly summarized below.

A 20 MeV/nucleon ^{197}Au beam, produced by the K1200 cyclotron, interacted with a ^{90}Zr target of thickness 1.0 mg/cm^2 . (The target thickness was such

that the maximum energy loss of the beam in traversing the target was 0.26 MeV/nucleon [39].) The reaction products were analyzed with the A1200 fragment separator operated in the medium acceptance mode [with an angular acceptance of 0.8 msr ($\Delta\theta = 20$ mr, $\Delta\phi = 40$ mr) and a momentum acceptance of 3%]. The primary beam struck the target at an angle of 1.0° relative to the optical axis of the spectrometer. The A1200 provided two intermediate dispersive images and a final achromatic image (focal plane). At the focal plane, the fragments were collected in a three-element (ΔE_1 , ΔE_2 , E) Si surface barrier detector telescope. The 300 mm² Si detectors were 50, 50 and 300 μm thick, respectively.

Time of flight was measured between a parallel plate avalanche counter (PPAC) and a microchannel plate detector (mcp) positioned at the first dispersive image and at the focal plane, respectively, and separated by a distance of 14 m. The PPAC at the first dispersive image was also X–Y position sensitive and used to record the position of the reaction products. The horizontal position, along with NMR measurements of the A1200 dipole fields, was used to determine the magnetic rigidity $B\rho$ of the particles. A series of measurements at overlapping magnetic rigidity settings of the spectrometer were performed in the region 1.500–1.750 Tesla-meters. This region is below the rigidity $B\rho=1.824$ T m of elastically scattered 20 MeV/nucleon ^{197}Au particles at their equilibrium charge state ($Q_{eq}=69.5$) [40].

The reaction products were characterized by an event-by-event measurement of dE/dx , E, time of flight, and magnetic rigidity. The response of the spectrometer/detector system to ions of known atomic number Z, mass number A, ionic charge q and velocity was measured using analog beams as described previously [7]. The procedure to extract Z, q and A from the measured quantities is outlined below and described in more detail in [7].

The transmission detectors (ΔE_1 and ΔE_2) were calibrated by directly correlating pulse height with energy loss as calculated using the data of Hubert et al. [39]. For the stopping (E) detector, pulse-height defect (PHD) corrections were necessary to obtain an accurate reconstruction of the residual energy of the particles. The procedure developed in [7] was used. The total energy E_{tot} of the particles entering the spectrometer (i.e. the sum of the energies deposited in the Si detectors plus small corrections due to the presence of the PPACs and mcp) had an overall resolution (FWHM) of 1.1%. The velocity resolution was about 0.5%.

The determination of the atomic number Z was based on the energy loss of the particles in the first ΔE detector and their velocity and was reconstructed using the expression:

$$Z = a_0(v) + a_1(v) v\sqrt{\Delta E} + a_2(v)(v\sqrt{\Delta E})^2 \quad (1)$$

where v is the velocity of the ion entering the detector and ΔE the energy loss. In order to determine the functions $a_0(v)$, $a_1(v)$ and $a_2(v)$ in the velocity range of interest, we used the data of Hubert et al. [39] to obtain the coefficients of Eq. (1) for the Z range 25–85 and in the energy range 12–24 MeV/nucleon by applying a least-squares fitting procedure at each energy, in steps of 0.5 MeV/nucleon. The values of each coefficient at the various energies were then fitted with polynomial functions of velocity. The atomic number Z of the particles was reconstructed from the measured ΔE and v using Eq. (1) with a resulting resolution (FWHM) of 0.9 Z units for heavy residues ($A=160$ – 200) and 0.6 Z units for fission-like ($A=100$ – 140) residues.

The ionic charge q of the particles entering the A1200 was obtained from the total energy E_{tot} , the velocity and the magnetic rigidity according to the expression:

$$q = \frac{3.107}{931.5} \frac{E_{tot}}{B\rho(\gamma - 1)} \beta\gamma \quad (2)$$

where E_{tot} is in MeV, $B\rho$ in Tm, $\beta = v/c$ and $\gamma = 1/(1 - \beta^2)^{\frac{1}{2}}$. The measurement of the ionic charge q had a resolution of 0.7 and 0.5 q units for heavy and fission-like residues, respectively. Since the ionic charge must be an integer, we assigned integer values of q for each event by setting appropriate windows on each peak of the q spectrum (see below). Using the magnetic rigidity and velocity measurement, the mass-to-charge A/q ratio of each ion was obtained from the expression:

$$A/q = \frac{B\rho}{3.107\beta\gamma} \quad (3)$$

Now, combining the q determination with the A/q measurement, the mass A was obtained as:

$$A = q_{int} \times A/q \quad (4)$$

(q_{int} is the integer ionic charge determined as above) with an overall resolution (FWHM) of 1.0 and 0.7 A units, again for heavy and fission-like residues respectively.

The requirement that q be within ± 0.3 units of its corresponding integer value was applied to eliminate contributions of adjacent q values to the mass assignment. Similarly, the requirement that Z be within ± 0.3 units of its corresponding integer value was applied to avoid contributions of adjacent Z values to the distributions of a given element.

Combination and appropriate normalization of the data at the various magnetic rigidity settings of the spectrometer provided fragment distributions with respect to Z , A , q and velocity. Correction of missing yields caused by charge changing at the PPAC (positioned at the dispersive image) was performed as in [7], based on the equilibrium charge state prescriptions of Baron et. al. [40]. The distributions were then summed over all values of q . It should be pointed out, as mentioned previously, that the resulting distributions in Z, A and velocity are residue yield distributions at a reaction angle of 1° with an angular window of 1.1° , in the magnetic rigidity range 1.500–1.750 T m.

3 Results and Discussion

The extracted residue yield distributions, sorted by mass number A , atomic number Z , and velocity β ($\equiv v/c$), are shown in Figs. 1a, 1b and 1c, respectively. The yields have been normalized to beam current and target thickness and are given in mb in Fig. 1a. The A distributions are summed over all values of Z and β . The Z – A distributions are summed over all values of β , and finally, the β – A distributions are summed over all values of Z .

It is apparent from examining Figs. 1a and 1b that the spectrometer acceptance and resolution have distorted the fragment yield distributions. For example, it was not possible to cleanly separate the beam nuclei from quasielastic fragments. Therefore, products that were very close in mass number, atomic number and energy to the projectile were either not collected by the spectrometer or rejected in the analysis. As a result, a small subset of quasielastic events is displayed in Fig. 1. (The quasielastic events shown in Fig. 1 are very proton rich relative to the projectile nucleus, which is incorrect. Their yields are greatly reduced compared to other fragments which is also incorrect.) We have chosen therefore to focus on the non-quasielastic events ($A \leq 160$) in the analysis.

The mass yield curve (Fig. 1a), has two humps, the distorted quasielastic one peaking at $A=193$ and the other extending from $A=170$ down to $A=80$. The second bump in the mass yield distribution consists of two groups of fragments (as can be deduced with the aid of Fig. 1c); one group resulting from modest ($\sim 15\%$) momentum transfer events with $A=120$ – 160 (heavy residues) and another group with $A=90$ – 120 and velocities of forward-moving fission fragments.

The radiochemical mass yield curves of target-like residues (and fission fragments) from the reactions 35 MeV/nucleon $^{84}\text{Kr}+^{197}\text{Au}$ [41] and 21 MeV/nucleon $^{129}\text{Xe}+^{197}\text{Au}$ [10] are also shown for comparison (solid and dashed lines, respectively). As noted earlier, due to the spectrometer acceptance, the measured

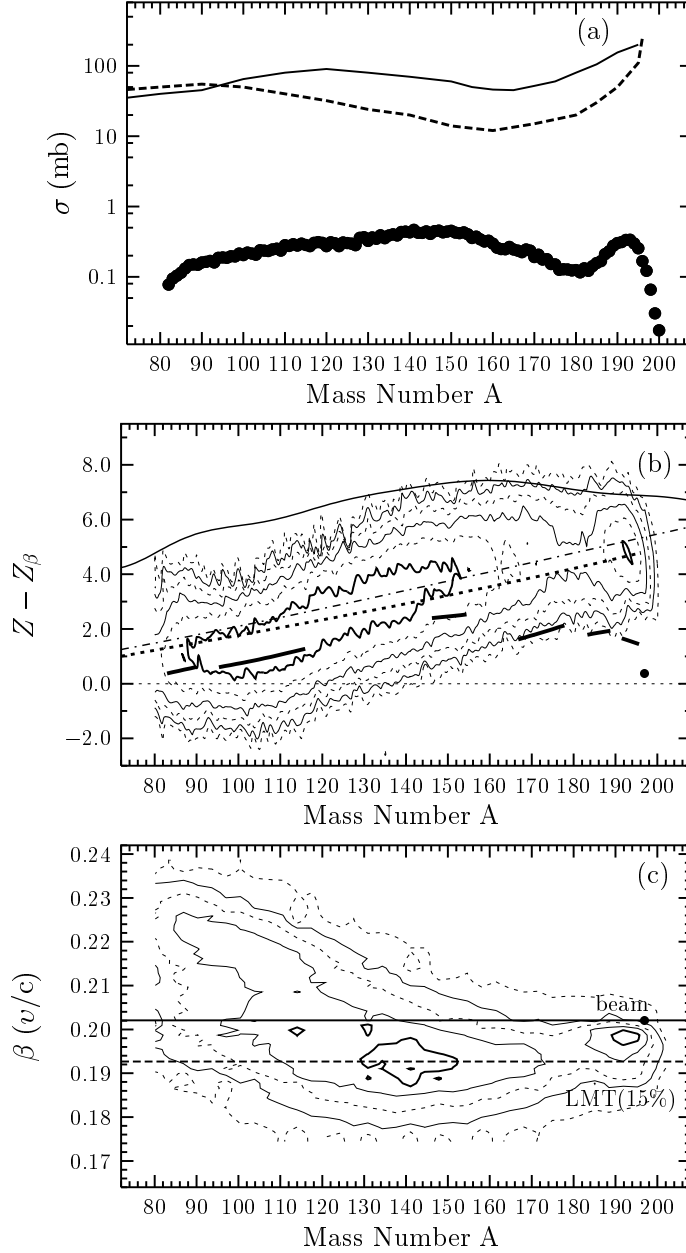


Fig. 1. Fragment distributions for the reaction of 20 MeV/nucleon ^{197}Au with ^{90}Zr . (a) isobaric yield distribution. The data are shown as solid points, whereas the solid and dashed lines indicate the yield curves from radiochemical measurements of the reactions 35 MeV/nucleon $^{84}\text{Kr}+^{197}\text{Au}$ [41] and 21 MeV/nucleon $^{129}\text{Xe}+^{197}\text{Au}$ [10], respectively. (b) yield distributions as a function of Z (relative to the line of β stability, Z_β) and A . Highest yield contours are plotted with thicker lines. Successive contours correspond to a decrease of the yield by a factor of 2. The dashed line indicates the expected values for intermediate energy projectile fragmentation [5], the dot-dashed line indicates the position of the modified “evaporation residue attractor line” [43] and the solid line indicates the position of the proton dripline for odd Z nuclei [44]. Finally, the thick line segments show the Z_p values obtained in the radiochemical measurements of 21 MeV/nucleon $^{129}\text{Xe}+^{197}\text{Au}$ [10]. (c) velocity vs. mass distributions. The definition of the velocity lines is as follows: horizontal full line: beam velocity; horizontal dashed line: velocity corresponding to 15% linear momentum transfer (LMT 15%).

yields, are much lower than the radiochemical cross sections and bear only scant resemblance to them.

In Fig. 1b, the yield distributions of the reaction products are shown as contour plots of Z versus A . The fragment Z is given relative to the line of beta-stability, Z_β , which was taken as $Z_\beta = A/(1.98 + 0.0155A^{2/3})$ [42]. The observed fragment distributions lie on the proton-rich side of stability ($Z - Z_\beta = 0$). Shown in Fig. 1b, are the centroids of the isobaric charge distributions from the radiochemical measurements of target-like fragments from the reaction 21 MeV/nucleon $^{129}\text{Xe} + ^{197}\text{Au}$ [10]. The radiochemical centroids for near-Au residues are close to stability due to the dominance of quasielastic events in this region. In the symmetric fission fragment region $A=90-120$, the centroids are in fair agreement with the present data, as they both correspond to fission fragments. In the region $A \sim 150$, the discrepancy may be due to a combination of experimental factors (e.g. limited number of measured nuclides in the radiochemical data and acceptance cut in the present data).

Also shown in Fig. 1b are the centroids of the Z distributions seen in intermediate energy projectile fragmentation [5]. Despite the fact that no fission is involved in these reactions, there is some similarity (but differences in the slope of Z vs A) between this prescription and the centroids of the yield distribution of the present data.

Charity [43] has recently discussed the concept of an “evaporation residue attractor line” (EAL). The EAL is a line in the $N-Z$ plane that represents the locus of fragment yields produced by the evaporation of neutrons and charged particles from highly excited nuclei. (The statistical model used to predict the position of the EAL is GEMINI). In Fig. 1b, we show the position of the modified heavy fragment EAL for the decay of highly excited heavy nuclei where the primary fragment is near the valley of beta stability. As shown in this figure, the centroids of the observed yields are similar to the modified EAL for this reaction ($A=80-160$), but the slope of Z vs A is not the same. This similarity in charge distributions for the products from the present reaction and the EAL for $A = 120-160$ indicates that these fragments are decay products of highly excited nuclei.

What causes the centroids of the contours in the data to become more n-rich compared to these two prescriptions as the fragment mass decreases? A possible answer is the occurrence of fission which produces more n-rich fragments than fragmentation (residue production). (The two empirical prescriptions [5,43] do not include the effects of fission.) The argument is that at $A=100$, a larger fraction of the fragments arise from fission (Fig. 1c) than at $A=150$, thus producing the observed slope of Z vs A . Evidence for this comes from comparison with the Z distributions measured radiochemically for the reaction of 20 MeV/nucleon Xe with Au, where the fission of the Au-like nucleus

is more prominent (Fig. 1a,1b). The observed centroids of the Z distributions for this reaction are more n-rich than the fragments observed in this work. (Fig. 1b). The definitive data comes from comparing Fig. 1b and 1c and noting that as fission (high velocity events) becomes more prominent, the charge distribution becomes more n-rich.

One does note that the contours of the observed yields in Fig. 1b lie close to the position of the proton dripline (plotted for odd Z nuclei [44]). Some of the observed products have 5–7 more protons than the stable isobar. To examine this point further, we show the detailed fragment charge distributions for selected A values for non-quasielastic fragments in Fig. 2.

For Fig. 2, an attempt has been made to correct the measured yields for the spectrometer angular acceptance, so that we may obtain estimates of fragment production cross sections, despite the fact that only a small fraction of the cross section was collected in the present measurements. Correction factors for the angular distributions of the fission-like fragments (A=90–160) were obtained assuming isotropic binary decay of the primary reaction product. For simplicity, this product was assumed to be a Au nucleus with velocity as this observed for the heavy residues (which, as already mentioned, correspond to $\sim 15\%$ linear momentum transfer) and was assumed to scatter off the target at an angle somewhat inside the grazing angle. (The grazing angle is 5.5° degrees and the scatter angle was taken to be 4.0° .) Typical correction factors were 40, 60, 90, 150 for masses A=160, 140, 120, 100, respectively. After applying mass-dependent correction factors to the measured yields, the resulting yields were normalized to values of cross sections of non-isomeric independent-yield nuclides from the radiochemical data of the reaction (21 MeV/nucleon) $^{129}\text{Xe}+^{197}\text{Au}$ [10]. Fragment production cross sections resulted with an estimated uncertainty of a factor of 2 (due to the correction procedure) and, for several A values, are presented in Fig. 2.

In examining Fig. 2, we are struck by the large number of nuclide yields measured for each mass number A, when compared to typical radiochemical measurements where, at best, the yields of two or three isobars are measured for each A value. The measured distributions appear to be rather broad. The general proton-rich character of these yield distributions indicates that these intermediate energy collisions may be useful for the synthesis of heavy proton-rich nuclei, complementary to the usual practice of synthesizing these nuclei via symmetric compound nuclear reactions involving the pxn exit channel [45]. An attempt to produce and identify proton emitting nuclei using the Au+Zr reaction is described in [46].

The velocity vs mass distributions (Fig. 1c) show the general absence of fusion-like collisions and the prevalence of dissipative collisions. As already mentioned, one also sees evidence for the occurrence of fission events for A=90–120

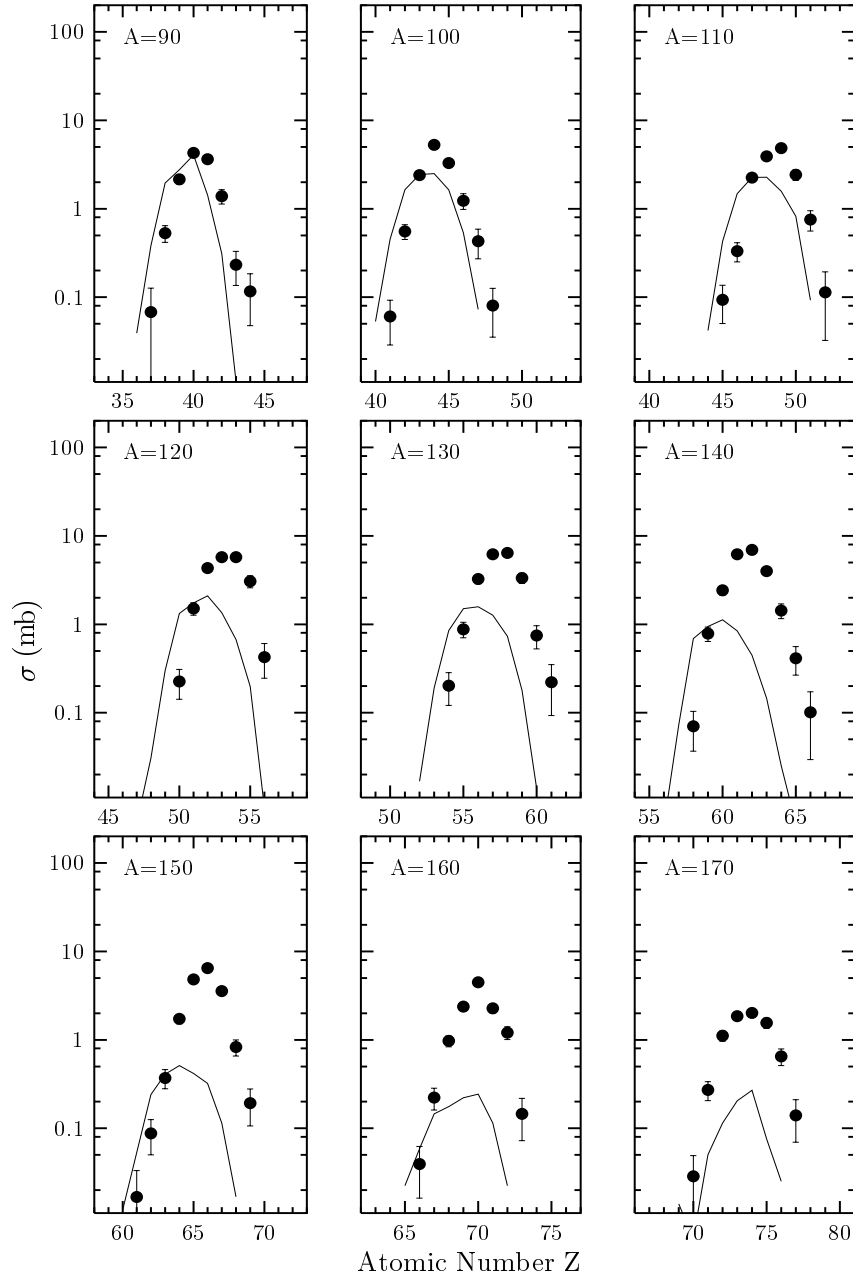


Fig. 2. Fragment charge distributions for selected values of the mass number A for the reaction of 20 MeV/nucleon ^{197}Au with ^{90}Zr . The data are shown as solid points. The full-line curves are calculations using the DIT+ICF code coupled to GEMINI (see text).

with velocities higher than that of the beam, corresponding to fission fragments moving forward in the rest frame of the fissioning nucleus (the spectrometer settings were such that only forward-moving fragments were collected from the two kinematical solutions). In addition, one sees a group of events ($A=120$ – 160) with rather constant velocity, lower than that of the beam (by approx. 5%) corresponding to $\sim 15\%$ fractional linear momentum transfer (FLMT).

The existence of a constant fragment velocity, roughly independent of fragment mass, is not consistent with fission, where the fragment velocity should be inversely correlated with the fragment mass (as it is for $A=90-120$ for the Au-like fragment) [47]. We associate this group of fragments ($A=120-160$) mainly with residues that have emitted one or more IMFs in accord with a recent radiochemical study of target-like residues from the ^{208}Pb (29 MeV/nucleon) + ^{197}Au reaction [48]. From the velocity of this group of fragments (relative to that of the beam) we can estimate an average total kinetic energy loss of ~ 350 MeV.

We also note in Fig. 1c, that the fragment group $A=90-120$, along with the fission fragments, contains residues characterized by constant velocity (as in the $A=120-160$ group). It is rather remarkable that residues with less than half the mass of the projectile nucleus are observed in this reaction.

4 Comparison with Reaction Simulations

To gain insight into the underlying reaction mechanisms, we have performed simulations using an appropriate phenomenological model. The basic features of the reaction mechanism model are pre-equilibrium emission, dissipative deep inelastic transfer (DIT) and for the most central collisions, an incomplete fusion component (ICF). The hybrid model we used that included these features has been described by Veselsky [49].

For each event corresponding to a given impact parameter (partial wave), the effect of pre-equilibrium emission was calculated using a variant of the exciton model. Then the interaction of the projectile and target nuclei are simulated using the Tassan-Got/Stephan model [50] for deep inelastic transfer assuming stochastic nucleon exchange (in the region of orbital angular momentum $\ell = 300-870$). For trajectories where the overlap between projectile and target nuclei exceeds 3 fm, it is assumed that incomplete fusion takes place with this mechanism being modeled using a variant of the abrasion-ablation model [51]. Following the creation of the primary fragments by this hybrid mechanism, the statistical de-excitation of the excited primary fragments was simulated using GEMINI [52]. The results of this calculation were then filtered by the angular and momentum acceptance of the spectrometer. This model has been used successfully [49] to describe the residues formed in the 35 MeV/nucleon $\text{Kr} + \text{Au}$ reaction [33,35] and the 20 MeV/nucleon $\text{Au} + \text{Ti}$ reaction studied by us [54].

Simulations were run for partial waves from $\ell=0-870$. De-excitation of the primary fragment distribution was done using GEMINI. This statistical deexcitation code uses Monte Carlo techniques and the Hauser-Feshbach formalism to

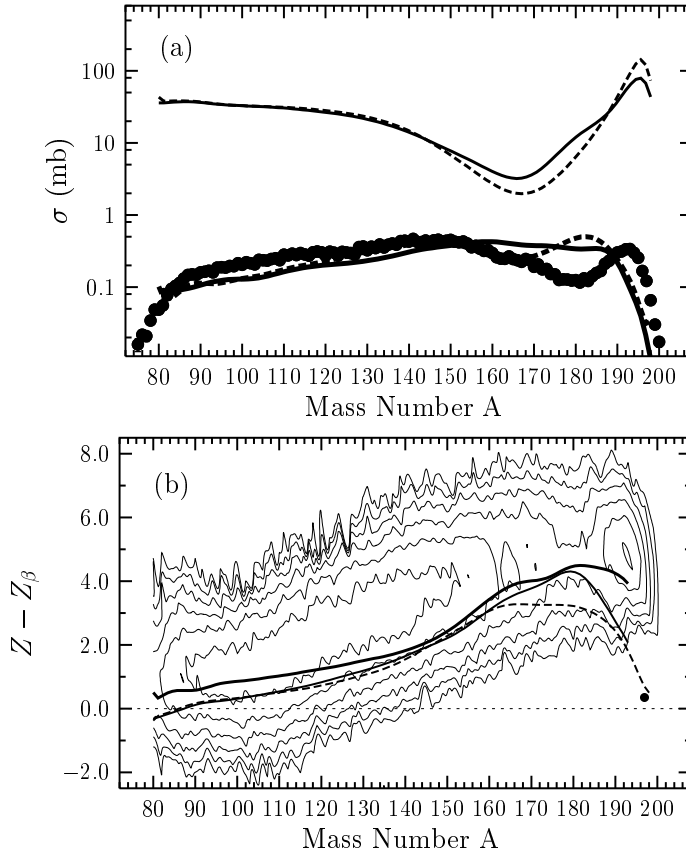


Fig. 3. Comparison of measured and calculated fragment distributions for the reaction of 20 MeV/nucleon ^{197}Au with ^{90}Zr . (a) isobaric yield distributions. The data are shown as solid points. The upper full line is the result of DIT+ICF/GEMINI calculation and the dashed line is from DIT/GEMINI (see text). The lower full line and dashed lines are the results of the same calculations as the upper ones, but with a cut corresponding to the angular and momentum acceptance of the spectrometer. (b) charge distributions. The data are shown as contours; the calculated values from DIT+ICF/GEMINI are shown as i) thick full line: with acceptance cut and, ii) thin full line: without acceptance cut, and the ones from DIT/GEMINI are shown as a dashed line (without acceptance cut).

calculate the probabilities for fragment emission with $Z \leq 2$. Heavier fragment and fission fragment probabilities are calculated using the transition state formalism of Moretto [53]. In the GEMINI calculations, we have used Lestone's temperature dependent level density parameter [55], a fading of shell corrections with excitation energy and we enabled IMF emission. Finally, fission delay was enabled with parameters as in [7]. Each partial-wave distribution was appropriately weighted and combined to give the overall fragment A , Z and velocity distributions (Figs. 3 and 4).

In Fig. 3a, we compare the measured and calculated mass yield curves for a number of conditions. The calculations were performed neglecting small

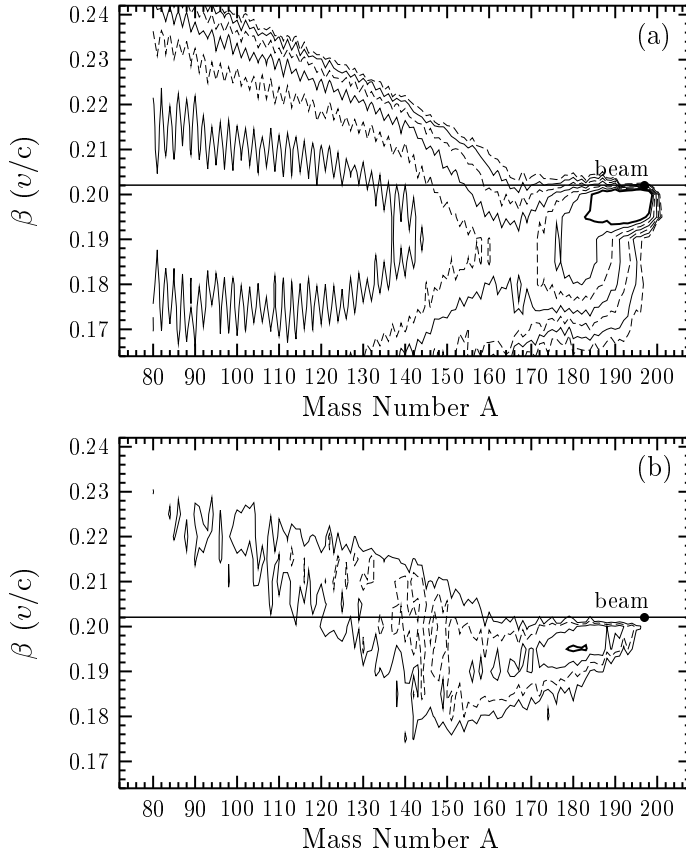


Fig. 4. The calculated (DIT+ICF/GEMINI) fragment velocity distributions (a) without and (b) with the spectrometer acceptance cut included in the calculation.

impact parameters (deep inelastic transfer only, DIT/GEMINI) or including all impact parameters (DIT+ICF/GEMINI). The upper dashed line is from DIT/GEMINI calculation and the upper solid line is from DIT+ICF/GEMINI calculation (without filtering with the spectrometer acceptance). The corresponding lower curves are from the same calculations in which filtering with the spectrometer acceptance has been performed. As we see, the shape of the mass yield curve is significantly altered by the overall spectrometer cut. Note however, the similarity of shapes between the measured yield curve and the calculated yield curves filtered with the spectrometer acceptance.

In Fig. 3b, the measured Z vs A yield distribution is compared with the predicted positions of Z_p , the most probable fragment atomic number for a given A value (given with respect to the line of β stability). Displayed are the results of DIT/GEMINI (dashed line, no acceptance filter), and of DIT+ICF/GEMINI (no acceptance filter: thin solid line, with spectrometer acceptance filter: thick line). We observe that the latter calculation with the acceptance cut does a fair job in describing the Z_p values of the $A=160-190$ residues, but predicts more n-rich fragments, consistent with fission, in the region $A < 160$. Thus, the heavy residue group $A=120-160$ seen in the data is not predicted by the

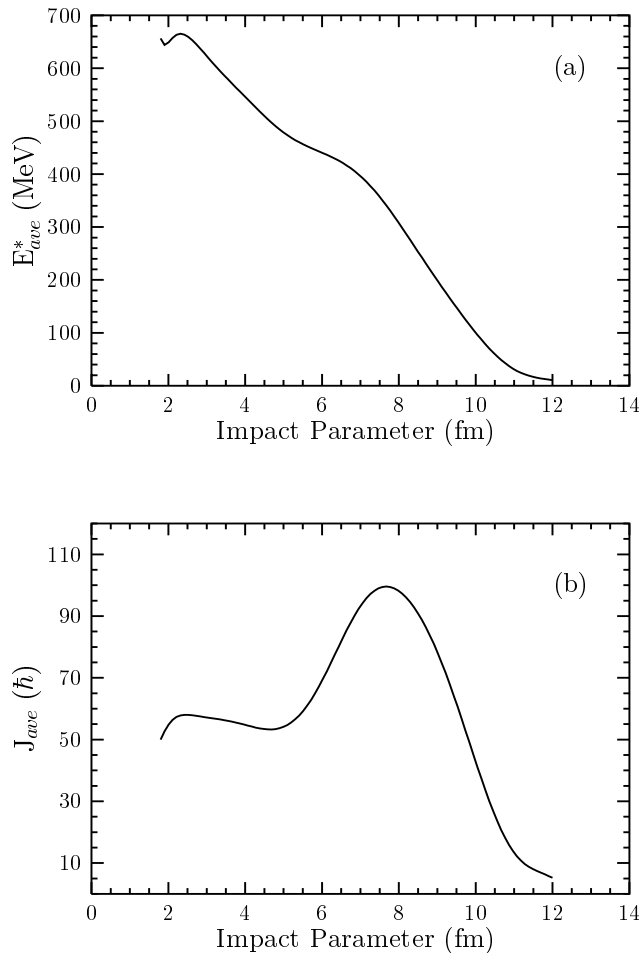


Fig. 5. The calculated (DIT+ICF/GEMINI) primary fragment mean excitation energy (a) and angular momenta (b) as a function of impact parameter for the reaction of 20 MeV/nucleon ^{197}Au with ^{90}Zr .

calculation, due to the prevalence of fission as a deexcitation channel in the GEMINI calculation.

The calculated fragment charge distributions are compared with the data in Fig. 2. The calculated centroids of the distributions are too n-rich as noted above, but the predicted widths of the charge distributions agree rather well with the observations.

In Fig. 4, we show the predicted velocity distributions (which are to be compared to Fig. 1c). In Fig. 4a, we show the unfiltered velocity distribution, while in Fig. 4b we show the velocity distribution as filtered by the spectrometer angular and momentum acceptance. Qualitatively, some features of the measured distributions are reproduced, i.e., the appearance of residue events ($A = 160\text{--}190$) with mean velocities similar to the observed velocities and the characteristic forward moving fission fragment velocity pattern for the

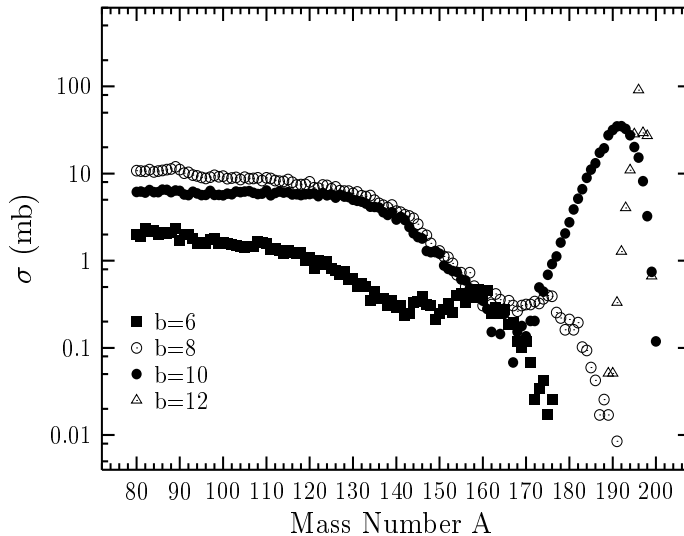


Fig. 6. The calculated (DIT+ICF/GEMINI) fragment mass distributions corresponding to selected values of the impact parameter b (in fm) for the reaction of 20 MeV/nucleon ^{197}Au with ^{90}Zr .

lighter fragments ($A < 120$) which are also similar to the observations. However, as already pointed out, the predicted velocities of the $A=120$ – 160 group are inversely correlated with mass and (along with their average Z values) are consistent with fission, whereas the measured properties of this fragment group are those of residues.

We conclude that the hybrid model proposed by Veselsky, coupled to a modern statistical de-excitation code, can describe some gross features of the residue distributions, especially those not too far from the projectile nucleus, whereas for lower mass residues it predicts mostly fission. We might then ask what we might learn about residue formation from the simulation model only. To gain insight regarding the primary interaction stage, we show in Fig. 5 the simulated properties (DIT+ICF/GEMINI) of the collision as a function of impact parameter b . Very large excitation energies and angular momenta are involved in these collisions. Interestingly, the average spin of products in the impact parameter range 6–8.5 fm is predicted to be higher than the maximum angular momentum for which the symmetric fission barrier vanishes (approx. $80\hbar$) which causes these nuclei to fission.

In Fig. 6, we show the simulated fragment mass distributions arising from collisions with various impact parameters. From these impact parameter sorted mass distributions, we see that the near projectile fragments originate in very peripheral collisions (quasielastic events) with (Fig. 5) low associated excitation energies and angular momenta. The rest of the fragments are produced by collisions involving a large range of impact parameters (and thus the fragment mass number A cannot be used as an impact parameter trigger). These

broad mass distributions represent events where the heavy fragment from the collision either fissioned symmetrically ($A=90-120$) or fissioned very asymmetrically or emitted one or more IMFs in its de-excitation ($A=120-160$). As already mentioned, the measured velocity spectra (Fig. 1c) indicate that these fragments ($A=120-160$) are not the result of symmetric fission.

5 Conclusions

What have we learned from this high resolution experimental study of the residues produced in the reaction 20 MeV/nucleon $^{197}\text{Au} + ^{90}\text{Zr}$? Two findings seem of particular importance. They are: (a) the observation of surviving residues ($A=120-160$) which appear to result from “hard collisions”. They are relatively neutron-deficient with broad charge distributions and velocity, on average, corresponding to a linear momentum transfer of $\sim 15\%$. (b) A semi-quantitative description of heavy residue formation in intermediate energy collisions between massive nuclei by the hybrid model of Veselsky followed by the statistical deexcitation code GEMINI was found. However, the calculation was not able to describe the residue group with $A=120-160$, and gave primarily fission fragments in the whole mass range $A < 160$.

We gratefully acknowledge the support of the A1200 group and operations staff of Michigan State University during the measurements and the help of L. Hart in the analysis of the data. One of us (G.A.S) is also thankful to M. Veselsky for his help in the course of calculations and stimulating discussions. Financial support for this work was given, in part, by the U.S. Department of Energy under Grant No. DE-FG06-88ER40402, No. DE-FG03-97ER41026, and Contract DE-AC03-76SF00098 and the National Science Foundation under Grant No. PHY-95-28844.

References

- [1] K. Aleklett, M. Johansson, L. Sihver, W. Loveland, H. Groening, P.L. McGaughey, and G.T. Seaborg, Nucl. Phys. A149 (1989) 591.
- [2] W. Loveland, K. Aleklett, L. Sihver, Z. Xu, C. Casey, D.J. Morrissey, J.O. Liljenzin, M. de Saint-Simon and G.T. Seaborg, Phys. Rev. C41 (1990) 973.
- [3] D. Bazin, D. Guerreau, R. Anne, D. Guillemand-Mueller, A.C. Mueller, and M.G. Saint-Laurent, Nucl. Phys. A515 (1990) 349.
- [4] B. Faure-Ramstein, F. Auger, J.P. Wieleczko, W. Mittig, A. Cunsolo, A. Foti, E. Plagnol, J. Quebert, and J.M. Pascaud, Nucl. Phys. A586 (1995) 533.

- [5] R. Pfaff, D.J. Morrissey, W. Benenson, M. Fauerbach, M. Hellstrom, C.F. Powell, B.M. Sherrill, M. Steiner, and J.A. Winger, *Phys. Rev.* C53 (1996) 1753.
- [6] K.A. Hanold, et al., *Phys. Rev.* C52 (1995) 1462.
- [7] G.A. Souliotis, K. Hanold, W. Loveland, I. Lhenry, D.J. Morrissey, A.C. Veeck, and G.J. Wozniak, *Phys. Rev.* C57 (1998) 3129.
- [8] O. Granier, et al., *Nucl. Phys.* A481 (1988) 109.
- [9] H. Barz, J.P. Bondorf, C.H. Dasso, R. Donangelo, G. Pollarolo, H. Schulz, and K. Sneppen, *Phys. Rev.* C46 (1992) R42.
- [10] A. Yokoyama, W. Loveland, J.O. Liljenzin, K. Aleklett, D.J. Morrissey, and G.T. Seaborg, *Phys. Rev.* C46 (1992) 647.
- [11] A.A. Marchetti, et al., *Phys. Rev.* C48 (1993) 266.
- [12] M. Aboufirassi, et al., LPCC 93-14, September, 1993; J.F. LeColley, et al., *Phys. Lett.* B325 (1994) 317.
- [13] E.J. Garcia-Solis, A.C. Mignerey, H. Madani, A.A. Marchetti, D.E. Russ, and D. Shapira, *Phys. Rev.* C52 (1995) 3114.
- [14] S.P. Baldwin, et al., *Phys. Rev. Lett.* 74 (1995) 1299.
- [15] M. Morjean, et al., *Nucl. Phys.* A591 (1995) 371.
- [16] D.G. d'Enterria, F. Fernandez, E. Laguera, M. Debeauvais, J. Ralarosy, S. Jokic, M. Zamani, and J. Adloff, *Phys. Rev.* C52 (1995) 3179.
- [17] J. Toke, et al., *Nucl. Phys.* A583 (1995) 519.
- [18] R.J. Otto, G.T. Seaborg, and M.M. Fowler, *Phys. Rev.* C17 (1978) 1071.
- [19] M. Rajagopalan, L. Kowalski, D. Logan, M. Japlan, J.M. Alexander, M.S. Zisman, and J.M. Miller, *Phys. Rev.* C19 (1979) 54.
- [20] D. Dalili, et al., *Z. Phys.* A316 (1984) 371.
- [21] D. Dalili, et al., *Z. Phys.* A320 (1985) 349.
- [22] G. Rudolf, et al., *Phys. Lett.* 57 (1986) 2905.
- [23] D. Dalili, et al., *Nucl. Phys.* A454 (1986) 163.
- [24] R. Lucas, et al., *Nucl. Phys.* A464 (1987) 172.
- [25] H. Solbach, H. Freiesleben, W.F.W. Schneider, D. Schull, P. Braun-Munzinger, B. Kohlmeyer, M. Marinescu, and F. Puhlhofer, *Nucl. Phys.* A467 (1987) 349.
- [26] W. Loveland, K. Aleklett, L. Sihver, Z. Xu, C. Casey, and G.T. Seaborg, *Nucl. Phys.* A471 (1987) 175c.

- [27] K. Aleklett, W. Loveland, M. de Saint-Simon, L. Sihver, J.O. Liljenzin, and G.T. Seaborg, *Phys. Lett B*236 (1990) 404.
- [28] M. Zamani, M. Debeauvais, J. Ralarosy, J.C. Adloff, F. Fernandez, S. Jokic, and D. Sampsonides, *Phys. Rev. C*42 (1990) 331.
- [29] A. Adorno, A. Bonasera, M. Avinato, M. Colonna, A. Cunsolo, G.C. DiLeo, M. DiToro, and F. Gulminelli, *Nucl. Phys. A*529 (1991) 565.
- [30] L. Stuttge, et al., *Nucl. Phys. A*539 (1992) 511.
- [31] B. Lott, et al., *Z. Phys. A*346 (1993) 201.
- [32] G.F. Peaslee, et al., *Phys. Rev. C*49 (1994) R2271.
- [33] W. Skulski., et al., in *Advances in Nuclear Dynamics*, W. Bauer, A. Mignerey, eds., (Plenum, New York, 1996) pp 21–30.
- [34] J. Colin, G. Bizard, A. Genoux-Lubain, C. LeBrun, J.F. LeColley, M. Louvel, Ch. Meslin, G. Rudolf, and L. Stuttge, *Nucl. Phys. A*583 (1995) 449.
- [35] B. Djerroud et al., *Phys. Rev. C*64 (2001) 034603; W. Skulski, et al., *Phys. Rev. C*53 (1996) R2594.
- [36] W.Q. Shen, et al., *Phys. Rev. C*57 (1998) 1508.
- [37] B. M. Sherrill, D. J. Morrissey, J. A. Nolen and J. A. Winger, *Nucl. Instrum. Methods B*56/57 (1991) 1106.
- [38] W.W. Wilcke et al., *At. Data Nucl. Data Tables* **25**, 389 (1980).
- [39] F. Hubert, R. Bimbot and H. Gauvin, *Atom. Data and Nucl. Data Tables* 46 1 (1990) and *Nucl. Instrum. Methods B*36 (1989) 357.
- [40] E. Baron, M. Bajard and Ch. Ricaud, *Nucl. Instrum. Methods A*328 (1993) 177.
- [41] W. Loveland, K. Aleklett, L. Sihver, Z. Xu, C. Casey and G.T. Seaborg, *Nucl. Phys. A*471 (1987) 175c.
- [42] P. Marmier and E. Sheldon, *Physics of Nuclei and Particles, Volume I* (Academic, New York, 1970) p. 15.
- [43] R.J. Charity, *Phys. Rev. C*58 (1998) 1073.
- [44] P. Moller, J.R. Nix, and K.L. Kratz, *At. Data and Nucl. Data Tables* 66 (1997) 131.
- [45] C. N. Davids, et al., *Phys. Rev. Lett.* 76 (1996) 592.
- [46] G.A. Souliotis, *Physica Scripta T*88 (2000) 153.
- [47] D. Dalili, et al., *Nucl Phys. A*454 (1986) 163.

- [48] W. Loveland, M. Andersson, K. E. Zyromski, N. Ham, B. Altschul, J. Vlcakova, D. Menge, J. O. Liljenzin, R. Yanez, and K. Aleklett, Phys. Rev. C59 (1999) 1472.
- [49] M. Veselsky, submitted in Nucl. Phys A., also see xxx.lanl.gov/abs/nucl-th/0107062.
- [50] L. Tassan-Got, and C. Stefan, Nucl. Phys. A524 (1991) 121.
- [51] J. Gosset, et al., Phys. Rev. C16 (1977) 629.
- [52] R. Charity, et al., Nucl. Phys. A483 (1988) 391. The version of GEMINI included modifications made up to July, 1998.
- [53] L.G. Moretto, Nucl. Phys. A247 (1975) 211.
- [54] G.A. Souliotis, W. Loveland, G.J. Wozniak, and K. Hanold, in Nuclear Chemistry Progress Report, Oregon State University, August 1998, pp 30–35.
- [55] J. Lestone, Phys. Rev. C52 (1995) 118.